

Muonic atoms and the nuclear structure

A. Antognini* for the CREMA collaboration

Institute for Particle Physics, ETH, 8093 Zurich, Switzerland

Laboratory for Particle Physics, Paul Scherrer Institute, 5232 Villigen-PSI, Switzerland

**E-mail: aldo.antognini@psi.ch*

High-precision laser spectroscopy of atomic energy levels enables the measurement of nuclear properties. Sensitivity to these properties is particularly enhanced in muonic atoms which are bound systems of a muon and a nucleus. Exemplary is the measurement of the proton charge radius from muonic hydrogen performed by the CREMA collaboration which resulted in an order of magnitude more precise charge radius as extracted from other methods but at a variance of 7 standard deviations. Here, we summarize the role of muonic atoms for the extraction of nuclear charge radii, we present the status of the so called “proton charge radius puzzle”, and we sketch how muonic atoms can be used to infer also the magnetic nuclear radii, demonstrating again an interesting interplay between atomic and particle/nuclear physics.

Keywords: Proton radius; Muon; Laser spectroscopy, Muonic atoms; Charge and magnetic radii; Hydrogen; Electron-proton scattering; Hyperfine splitting; Nuclear models.

1. What atomic physics can do for nuclear physics

The theory of the energy levels for few electrons systems, which is based on bound-state QED, has an exceptional predictive power that can be systematically improved due to the perturbative nature of the theory itself [1, 2]. On the other side, laser spectroscopy yields spacing between energy levels in these atomic systems so precisely, that even tiny effects related with the nuclear structure already influence several significant digits of these measurements. Thus, highly accurate atomic transition frequency measurements can be used as precise and clean probes (purely electromagnetic interaction) of low energy-QCD properties of the nucleus due to the low energy nature of the photons articulating the interaction between the nucleus and the orbiting particle.

A particular class of atoms, called muonic atoms, offer an interesting opportunity to extract properties of the nucleus with high accuracy. In these atoms, one or more electrons are substituted by a muon, which is a fundamental particle having the same electromagnetic properties as the electron but with a much larger mass ($m_\mu \approx 200m_e$). For example muonic hydrogen (μp) is the bound system of a negative muon and a proton, muonic helium ion (μHe^+) a muon bound to an alpha particle. The atomic properties are strongly affected by the orbiting particle mass m , e.g., the Bohr energy scales linearly with m while the Bohr radius as $1/m$, resulting already for low- Z atoms in muonic binding energies of several keV and in a so strong overlap of the muon wave functions with the nucleus that the energy

levels are considerably (%-level) affected by the nucleus finite size. A paradigmatic example is μp whose laser spectroscopy yielded a very precise determination of the proton charge radius [3, 4].

2. Charge and magnetic radii of the proton from scattering

The scattering process between charged particles without internal structure, as for example electron-electron scattering can be fully described within QED. Oppositely, when describing electron-proton scattering, form factors need to be introduced to parameterize the complexity of the nuclear structure. They contain dynamical information on the electric and magnetic currents in the nucleus defining the response to the electromagnetic fields. As a consequence of current conservation and relativistic invariance, for the spin-1/2 nuclei, as protons, only two form factors are required. Experimentally these form factors can be accessed through measurements of the elastic differential cross section which in the one-photon approximation is [5]

$$\left(\frac{d\sigma}{d\Omega}\right)_{\text{elastic}} = \left(\frac{d\sigma}{d\Omega}\right)_{\text{Mott}} \times \frac{1}{1+\tau} \left(G_E^2(Q^2) + \frac{\tau}{\epsilon} G_M^2(Q^2)\right), \quad (1)$$

where the Mott cross section applies for point-like particles and is fully calculated in the QED framework. $G_E(Q^2)$ and $G_M(Q^2)$ are the electric and magnetic Sachs form factors, while $\tau = Q^2/4M^2$ and $\epsilon^{-1} = 1 + 2(1+\tau)\tan^2(\theta/2)$ are kinematical variables with θ being the electron scattering angle and M the nucleus mass. At $Q^2 = 0$ the form factors correspond to the total charge in units of e and magnetic moment in units of the proton magneton: for the proton $G_E^p(0) = 1$ and $G_M^p(0) = 2.793$. So in first approximation at low momentum exchange the response of the nucleus to electromagnetic fields is ruled by its charge and magnetic moment.

Viewed as a Taylor series the charge and the magnetic moment are the first terms in an infinite list of parameters which describes the interaction of the proton with the electromagnetic fields [6]. The next parameters would be the slopes of the electric and magnetic form factors at zero momentum exchange:

$$R_E = -\frac{6}{G_E(0)} \frac{dG_E}{dQ^2} \Big|_{Q^2=0} \quad \text{and} \quad R_M = -\frac{6}{G_M(0)} \frac{dG_M}{dQ^2} \Big|_{Q^2=0}. \quad (2)$$

These equations represent the covariant definition of charge and magnetic radii, which in a non-relativistic approximation correspond to the second moments of the electric charge and magnetization distributions ρ_E and ρ_M of the nucleus

$$R_{E/M}^2 \approx \int d\vec{r} \rho_{E/M}(\vec{r}) r^2. \quad (3)$$

Any hadron/nuclear theory must reproduce these radii being parameters as fundamental as the charge, mass and magnetic moment. Although lattice QCD shows an impressive progress [7], currently these radii can not be accurately predicted from ab-initio theories and their knowledge relies on experiments [5, 8].

The traditional way to extract the form factors from the measured differential cross sections is based on the Rosenbluth separation techniques which consist in plotting the reduced cross section σ_{red} versus ε :

$$\sigma_{\text{red}} \equiv \frac{\varepsilon(1+\tau)}{\tau} \frac{\left(\frac{d\sigma}{d\Omega}\right)_{\text{elastic}}}{\left(\frac{d\sigma}{d\Omega}\right)_{\text{Mott}}} = G_M^2 + \frac{\varepsilon}{\tau} G_E^2. \quad (4)$$

The reduced cross section is linear in ε , with the slope proportional to G_E^2 and the intercept equal to G_M^2 . So both form factors can be deduced by measuring $\left(\frac{d\sigma}{d\Omega}\right)_{\text{elastic}}$ at several values of ε which is achieved by varying the electron beam energy and the electron scattering angle while keeping Q^2 fixed.

After this G_E/G_M separation, each measured form factor can be fitted with a polynomial expansion of the form [9]

$$G_{E/M}(Q) = G_{E/M}(0) \left[1 - \frac{Q^2}{6} \langle r_{E/M}^2 \rangle + \frac{Q^4}{120} \langle r_{E/M}^4 \rangle - \dots \right], \quad (5)$$

where $\langle r_{E/M}^N \rangle$ represent the N -th moments of the charge/magnetic distributions ($\langle r_{E/M}^2 \rangle = R_{E/M}^2$). At very low Q^2 , one could hope that the higher moments terms are sufficiently small, such that the $\langle r_{E/M}^2 \rangle$ -term can be determined without using a specific model for the form factor. However, at low Q^2 also the $\langle r_{E/M}^2 \rangle$ -term becomes increasingly small relative to the first term of the expansion resulting in a loss of sensitivity. So in practice to fit the measured form factors and extract the radii it is necessary to include data at intermediate Q^2 . As cross sections data are available only down to a minimal Q^2 , and because an extrapolation to $Q^2 = 0$ is required, the choice of the fit function (form factor model) is very important.

This extrapolation is even more challenging for the magnetic radii because of the ε/τ -dependence in Eq. (1) which results in an additional suppression of sensitivity (at low Q^2) of the measured cross sections to G_M compared to G_E . Consequently, the increased uncertainties of G_M at low Q^2 yields magnetic radii with larger uncertainties relative to charge radii. This calls for alternative determinations of the magnetic radii such as from polarized-recoil scattering [5] or atomic spectroscopy.

3. Charge and magnetic radii of the proton from atomic physics

The finite radius of the nucleus implies that its charge is smeared over a finite volume. For hydrogen-like S-states there is a non-negligible probability that the “orbiting” particle is spending some time inside the nuclear charge distribution, thus experiencing a reduced electrostatic attraction as compared to a point-like nucleus. This reduced attraction caused by the modification of the Coulomb potential for very small distances is giving rise to a shift of the atomic energy levels which for S-states H-like systems in leading order reads [1, 2]

$$\Delta E_{\text{finite size}} = \frac{2\pi Z\alpha}{3} |\phi^2(0)|^2 R_E^2 = \frac{2m_r^3 (Z\alpha)^4}{3n^3} R_E^2, \quad (6)$$

where $\phi(0)$ is the wave function at the origin in coordinate space, $m_r = mM/(m + M)$ the reduced mass of the atomic system with m being the orbiting particle mass, and M the nucleus mass, α the fine structure constant, Z the charge number of the nucleus and n the principal quantum number.

The m_r^3 dependence of Eq. (6) reveals the advantages related with muonic atoms. As the muon mass is 200 times larger than the electron mass, the muonic wave function strongly overlaps with the nucleus ensuing a large shift of the energy levels due to the nuclear finite size. Thus, the muonic bound-states represent ideal systems for the precise determination of nuclear charge radii R_E [3, 4, 10].

Because of this sensitivity to the finite size a moderate (20 ppm) accuracy in the measurement of the 2S-2P transition in μp is sufficient to extract the proton charge radius very accurately (5×10^{-4} relative accuracy) [3, 4]. In regular H, the accuracies of the transition frequency measurements, also relative to the line-widths, have to be much higher (see Table 1) to compete with this value. By combining in a least-square adjustment all high-precision frequency measurements in H available to date, as accomplished by the CODATA group, a proton charge radius with an accuracy of about 1% is obtained.

Atomic spectroscopy can be used also to extract magnetic radii. This is achieved through precision measurement of hyperfine splittings [4, 11, 12]. For H-like systems, in leading approximation the HFS is given by the magnetic interaction between the nucleus $\vec{\mu}_N$ and the orbiting particle $\vec{\mu}_m$ magnetic moments, described by [1, 2]

$$H \sim \vec{\mu}_N \cdot \vec{\mu}_m \delta(\vec{r}) , \quad (7)$$

which results in an energy splitting of the 1S state given by the Fermi energy

$$E_F = \frac{8}{3} \frac{Z^3 \alpha^4 m_r^3}{m M n^3} \mu_N . \quad (8)$$

The finite size correction to this splitting, which is of second order in perturbation theory, is [2, 12]

$$\Delta E_{\text{Zemach}} = -2(Z\alpha)m_r E_F R_Z \quad (9)$$

where the Zemach radius R_Z is defined as an integral of the charge and magnetic form factors

$$R_Z = -\frac{4}{\pi} \int_0^\infty \frac{dQ}{Q^2} \left(G_E(Q^2) \frac{G_M(Q^2)}{1 + \kappa_p} - 1 \right) , \quad (10)$$

(with κ_p the proton anomalous magnetic moment). In a non-relativistic approximation R_Z can be expressed, by the first moment of the convolution between charge and magnetic distributions $\rho_E(r)$ and $\rho_M(r)$ in coordinate space

$$R_Z = \int d^3\mathbf{r} |\mathbf{r}| \int d^3\mathbf{r}' \rho_E(\mathbf{r} - \mathbf{r}') \rho_M(\mathbf{r}'). \quad (11)$$

When assuming form factor models or using measured form factor data, the magnetic radius can be extracted from the Zemach radius. Thus, accurate measurements

of the HFS in μp and H can be used as complementary ways to obtain a precise value of the proton magnetic radius, or alternatively, as presented in [13] a self-consistent value of $R_E^2 + R_M^2$.

4. The proton charge radius puzzle

Three complementary routes to the proton charge radius have been undertaken: the historical method relies on elastic electron-proton scattering, the second one on high-precision laser spectroscopy in H, and the third one on high sensitivity laser spectroscopy in μp . The value extracted from μp [3, 4] with a relative accuracy of 5×10^{-4} is an order of magnitude more accurate than obtained from the other methods. Yet the value is 4% smaller than derived from electron-proton scattering [8, 14, 15] and H spectroscopy [17] with a disagreement at the 7σ level.

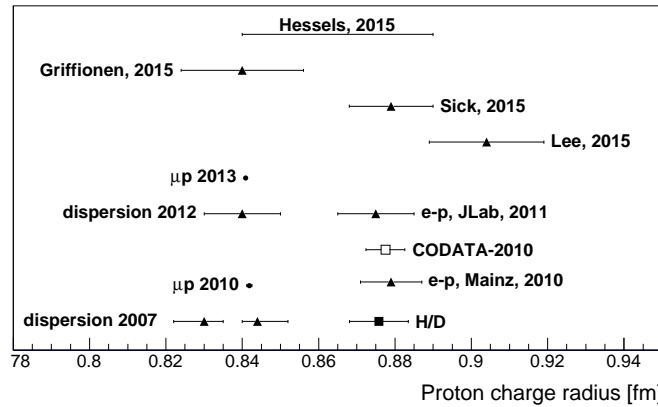


Fig. 1. Proton charge radii determined from spectroscopy of muonic atoms (full circles), from electron scattering (triangles) and from H/D spectroscopy (full squares).

The most recent evaluations of the proton charge radius are summarized in Fig. 1. The most precise values are extracted from two transition frequency measurements in μp . By combining them we obtained a $2S-2P_{1/2}$ splitting of $\Delta E_{2S-2P_{1/2}}^{\text{exp}} = 202.3706(23)$ meV equivalent to a frequency of 48932.99(55) GHz, limited by statistics while the systematic effects are at the 300 MHz level [4]. Equating this experimental value with the theoretical prediction

$$E_L^{\text{th}} = 206.0336(15) [\text{meV}] - 5.2275(10) \left[\frac{\text{meV}}{\text{fm}^2} \right] R_E^2 + 0.0332(20) [\text{meV}] \quad (12)$$

yields the proton charge radius R_E in fm. The first term of Eq. (12) accounts for QED contributions, the second one for finite size effects, and the third one for the two-photon exchange (TPE) contribution which is a second-order perturbation theory contribution related with the proton structure. In the last years as summarized in [10, 18, 19] various cross checks and refinements of bound-state QED and TPE

calculations needed for the extraction of R_E from μp have been performed, but no substantial missing effects have been found that could explain the discrepancy.

The typical systematics affecting the atomic energy levels are substantially suppressed in μp due to the stronger binding. The internal fields and the level separation of the muonic atoms are greatly enhanced compared to regular atoms making them insensitive to external fields (AC and DC Stark, Zeeman, black-body and pressure shifts). Thus μp turns out to be very sensitive to the proton charge radius (m_r^3 -dependence) and insensitive to systematics which typically scale as $\sim 1/m_r$.

Special attention was devoted to the analysis of electron-proton scattering data and the issues related with the extrapolation procedure. Starting from fit functions given by truncated general series expansions such as Taylor, splines and polynomials a large progress has been achieved in the last years by the use of various techniques: enforcing analyticity [6, 15], constraining the low Q^2 behavior of the form factor assuming a large- r behavior of the charge distribution [14] or by using proton models [20]. Tension exists between various electron-proton data analysis: some give results compatible with μp [20–22], some at variance [8, 14–16]. Because data at even lower Q^2 would facilitate the extrapolation at $Q^2 = 0$, two electron-proton experiments have been initiated, one at JLAB [23], the other one at MAMI Mainz [24]. A comparison between muon-proton and electron-proton scattering within the same setup as proposed by the MUSE [25] collaboration at PSI could disclose a possible violation of muon-electron universality.

Several “beyond standard model” BSM extensions have been studied but the majority of them have difficulties to resolve the discrepancy without conflicting with other low energy constraints. Still some BSM theories can be formulated but they require fine-tuning (e.g. cancellation between axial and vector components), targeted coupling (e.g. preferentially to muons) and are problematic to be merged in a gauge invariant way into the standard model [26, 27]. Breakdown of the perturbative approach in the electron-proton interaction at short distances, as well as the interaction with sea $\mu^+\mu^-$ and e^+e^- pairs and unusual proton structure have been suggested as possible explanation but without conclusive quantification [28].

Summarizing, currently the discrepancy persists even though recent reanalysis of scattering data have led to larger uncertainties of the extracted proton radius. New data from muonic deuterium and helium, from H spectroscopy and electron-proton scattering holds the potential to clarify the situation in the near future.

5. The proton radius from H spectroscopy

In a simplified way, the hydrogen S-state energy levels can be described by

$$E(nS) = \frac{R_\infty}{n^2} + \frac{L_{1S}}{n^3}, \quad (13)$$

where $R_\infty = 3.289\,841\,960\,355(19) \times 10^{15}$ Hz is the Rydberg constant and

$$L_{1S} \simeq 8171.636(4) \text{ [MHz]} + 1.5645 \left[\frac{\text{MHz}}{\text{fm}^2} \right] R_E^2 \quad (14)$$

the 1S Lamb shift given by bound-state QED contributions. The different n -dependence of the two terms in Eq. (13) permits to extract both R_∞ and L_{1S} (thus R_E) from at least two frequency measurements in H.

Being the most precisely known transition (relative accuracy of 4×10^{-15}) [29] and having the largest sensitivity to R_E , usually the 1S-2S transition is used. By combining it with a second transition measurement, R_∞ is eliminated and R_E can be extracted. When taken individually, the various R_E values extracted from H spectroscopy by combining two frequency measurements (2S-4S, 2S-12D, 2S-6S, 2S-6D, 2S-8S, 1S-3S as “second” transition [17]) are statistically compatible with the value from μp . Only the value extracted by pairing the 1S-2S and the 2S-8D transitions is showing a 3σ deviation while all the others differ only by $\lesssim 1.5\sigma$.

So the 4σ discrepancy between the proton charge radius from μp and H spectroscopy emerges only after an averaging process (mean square adjustments of all measured transitions) of the various “individual” determinations and consequently is less startling than it looks at first glance. A small systematic effect common to the H measurements could be sufficient to explain the deviation between μp and H results. This fact becomes even more evident if we consider the frequency shifts (absolute and normalized to the line-width) necessary to match the R_E values from μp and H, as summarized for selected transitions in Table 1. Obviously the discrepancy

Table 1. Relative accuracy of the various transition measurements in H, and hypothetical shift of the measured transition frequencies needed to match the R_E from H and μp . This shift is expressed also relative to the experimental accuracy σ , and to the transition effective line-widths Γ_{eff} .

Transition	Relative accuracy	Shift in σ	Shift in Hz	Shift in line-width
$\mu\text{p}(2\text{S}-2\text{P})$	2×10^{-5}	100σ	75 GHz	$4 \Gamma_{\text{eff}}$
H(1S-2S)	4×10^{-15}	$4'000 \sigma$	40 kHz	$40 \Gamma_{\text{eff}}$
H(2S-4P)	3×10^{-11}	1.5σ	9 kHz	$7 \times 10^{-4} \Gamma_{\text{eff}}$
H(2S-2P)	1×10^{-6}	1.5σ	5 kHz	$7 \times 10^{-4} \Gamma_{\text{eff}}$
H(2S-8D)	9×10^{-12}	3σ	20 kHz	$2 \times 10^{-2} \Gamma_{\text{eff}}$
H(2S-12D)	1×10^{-11}	1σ	8 kHz	$5 \times 10^{-3} \Gamma_{\text{eff}}$
H(1S-3S)	4×10^{-12}	1σ	13 kHz	$5 \times 10^{-3} \Gamma_{\text{eff}}$

can not be solved by slightly tuning (shifting) the measured values of the 1S-2S transition in H and the 2S-2P transitions in μp because it would require displacements corresponding to 4000σ and 100σ , respectively. Expressing the required frequency shift relative to the line-width as in the last column allows to better recognize some aspects of the experimental challenges. For example a shift of only $7 \times 10^{-4} \Gamma$ of the 2S-4P transition would be sufficient to explain the discrepancy. A control of the systematics which could distort and shift the line shape on this level of accuracy is far from being a trivial task. Well investigated are the large line broadening owing

to inhomogeneous light shifts which results in profiles with effective widths much larger than the natural line-widths [17].

Another exemplary correction relevant in this context, named quantum interference, has been brought recently back to attention [30], and has lead to various reevaluations of precision experiments. An atomic transition can be shifted by the presence of a neighboring line, and this energy shift δE , as a rule of thumb, amounts maximally to $\frac{\delta E}{\Gamma} \approx \frac{\Gamma}{D}$ where D is the energy difference between the two resonances and Γ the transition line-width. Thus, if a transition frequency is aimed with an absolute accuracy of Γ/x , then the influence of the neighboring lines with $D \leq x\Gamma$ has to be considered. The precise evaluation of these quantum interference effects are challenging because they require solving numerous differential equations describing the amplitude of the total excitation and detection processes from initial to final state distributions which depends on the details of the experimental setup.

Generally speaking, transition frequencies involving states with large n are more sensitive to systematic effects caused by external fields. Emblematic is the n^7 -dependence of the Stark effect. Motivated by the possibility that minor effects in H could be responsible for the discrepancy, various activities have been initiated in this field: at MPQ Garching the 2S-4P [31] and 1S-3S transitions are addressed, at LKB Paris the 1S-3S [32], and at the Toronto university the 2S-2P [33].

The “second” (beside the 1S-2S transition) transition frequency measurement in H can be interpreted as a R_∞ determination. Optical spectroscopy of H-like ions between circular Rydberg states where the nuclear size corrections are basically absent, the QED contributions small, and the line-widths narrow can be used as alternative determination of R_∞ [34]. Another way to R_∞ is through spectroscopy of muonium and positronium atoms which are purely leptonic systems where uncertainties related with the finite size are absent [35].

6. Hyperfine splitting in μp and $\mu^3\text{He}^+$

As a next step, we plan to prepare the measurement by means of laser spectroscopy of the ground state hyperfine splitting (1S-HFS) in μp and $\mu^3\text{He}^+$ with few ppm relative accuracy. Similar activities in μp exist at RIKEN-RAL and J-PARC [36, 37]. The theoretical prediction for the 1S-HFS in μp is approximately [11, 12, 38, 39]

$$\Delta E_{\text{HFS}}^{\text{th}} = 182.819(1) [\text{meV}] - 1.301 \left[\frac{\text{meV}}{\text{fm}} \right] R_Z + 0.064(21) [\text{meV}] , \quad (15)$$

where the first term includes the Fermi energy, QED corrections, hadronic vacuum polarization, recoil corrections and weak interactions. These contributions are known well enough. The second term is the finite size contribution, which is proportional to R_Z . It contains also some higher order mixed radiative finite-size corrections. The third term is given by the proton polarizability contribution.

By comparing the theoretical prediction with the experiment, it will become possible to deduce R_Z with a relative accuracy better than 5×10^{-3} provided that the polarizability contribution will be improved below 10% relative accuracy. This

contribution can be computed using a dispersive approach and measured proton polarized structure function g_1 and g_2 [38, 39] or via chiral perturbation theories (ChPT) [40]. An improvement of this contributions is conceivable in the near future due to the considerable advance in ChPT [41] and due to various ongoing measurements of the proton structure functions at JLAB using polarized target and beams.

For $\mu^3\text{He}^+$ the situation is conceptually similar to μp . The theoretical predictions assumes the same form as in Eq. (15) but with different numerical values.

The motivations for these experiments are several:

- **Bound-state QED in H and understanding of the 21 cm line**

The uncertainty of R_Z presently limits, together with the polarizability contribution, the theoretical prediction of the 1S-HFS in H. Therefore, the comparison between the experimental 1S-HFS value in H, which has a relative accuracy smaller than 10^{-12} , with the theoretical predictions is limited by the uncertainty of the proton structure contributions. This situation can be improved by complementary measurements in μp opening the way for a test of the HFS in H at the 10^{-7} level of accuracy.

- **Understanding of the proton structure**

Practically, from the Zemach radius the magnetic radius can be obtained by using form factor models or measured form factor data. As the determination of R_M from elastic electron-proton scattering is very challenging due to the loss of sensitivity for the magnetic form factor with decreasing momentum exchange, a precise measurement of R_Z from the muonic HFS represents a valuable complementary route to R_M . It can be used also to sort out a 8% discrepancy between R_M as extracted from the recent unpolarized electron-proton cross sections measurements in Mainz, and as deduced from polarized-recoil data at JLAB [6, 8, 15, 20].

Currently, we cannot determine the radii and the form factors accurately from theory, although lattice QCD is making impressive progress on this issue [7]. A precise measurement of R_Z from μp and its comparison with correlative measurements from scattering experiments bears the potential to push the frontier of our understanding of the complex non-perturbative nature of the proton structure which has been deeply reviewed in the last 15 years especially due to polarization data and the development of theoretical tools such as chiral perturbation theory.

The interplay between the muonic measurement and investigations of the proton structure can be articulated in several ways. As mentioned previously R_Z (R_M) represents a benchmark for the understanding of the proton structure. Extraction of a precise value for the Zemach radius from the μp 1S-HFS measurement requires the knowledge of the proton polarizability contribution which requires modeling of the proton and data from scattering (ChPT, g_1 and g_2 structure functions). Inverting this logic, a precise value of R_Z from scattering data [42] can be thus used, when paired with

the μp HFS, to check the polarizability contribution.

- **Nuclear physics from $\mu^3\text{He}^+$**

Nuclei like ^3He are calculable very precisely by a wide variety of ab-initio methods and so provide an important comparison between experiment and theoretical models of both the nuclear interactions (potential) and the electromagnetic currents [43]. The magnetic distribution and magnetic radii turn out to be very sensitive to the meson-exchange currents. A very hot topic in hadronic physics is to measure various parton distributions to see the quark spin distribution within protons and neutrons. The same should be done for nucleon spin distributions in nuclei.

7. Conclusions

Precision measurements in muonic atoms have triggered a plethora of theoretical works and experimental investigations in various fields of physics showing the potential and interdisciplinarity of these precision experiments [27]. Spectroscopy of the 2S-2P splittings in μp , μd , $\mu^3\text{He}^+$ and $\mu^4\text{He}^+$ has been accomplished by the CREMA collaboration. Besides the proton charge radius, soon new accurate values of the deuteron and ^3He and ^4He nuclear radii will be extracted from these measurements providing insights into the proton radius puzzle, and benchmarks to check few-nucleon ab-initio calculations. Moreover they can be used as anchor point for the ^6He - ^4He and ^8He - ^4He isotopic shift measurements [44] and their knowledge opens the way to enhanced bound-state QED tests for one- and two-electrons systems in “regular” He^+ [45] and He [46].

Spectroscopy of HFS transitions in μp and $\mu^3\text{He}^+$ provides a natural continuation of the CREMA program. Letting aside the proton radius puzzle related “new physics” searches the 1S-HFS in μp and $\mu^3\text{He}^+$ measurements impact three aspects of fundamental physics: bound-state QED in H-like systems, our understanding of the magnetic distributions and the low-energy spin structure of proton and ^3He nucleus.

Acknowledgments

This work is supported by the Swiss National Science Foundation Projects No. 200021L_138175 and No. 200020_159755. We acknowledge fruitful discussions with N. Barnea, R. Wiringa, I. Sick and V. Pascalutsa.

References

- [1] M. I. Eides, H. Grotch and V. A. Shelyuto, Theory of light hydrogenlike atoms, *Phys. Rep.* **342**, 63 (2001).
- [2] S. G. Karshenboim, Precision physics of simple atoms: QED tests, nuclear structure and fundamental constants, *Phys. Rep.* **422**, 1 (2005).
- [3] R. Pohl, A. Antognini, F. Nez et al., The size of the proton., *Nature* **466**, 213 (2010).

- [4] A. Antognini, F. Nez, K. Schuhmann et al., Proton Structure from the Measurement of 2S-2P Transition Frequencies of Muonic Hydrogen, *Science* **339**, 417 (2013).
- [5] V. Punjabi, C. F. Perdrisat, M. K. Jones, E. J. Brash and C. E. Carlson, The Structure of the Nucleon: Elastic Electromagnetic Form Factors, *arXiv:1503.01452* (2015).
- [6] Z. Epstein, G. Paz and J. Roy, Model independent extraction of the proton magnetic radius from electron scattering, *Phys. Rev. D* **90**, 074027 (2014).
- [7] J. R. Green, M. Engelhardt, S. Krieg, J. W. Negele, a. V. Pochinsky and S. N. Syritsyn, Nucleon structure from Lattice QCD using a nearly physical pion mass, *Phys. Rev. D* **90**, 074507 (2014).
- [8] J. Bernauer, M. Distler, J. Friedrich et al., Electric and magnetic form factors of the proton, *Phys. Rev. C* **90**, 015206 (2014).
- [9] I. Sick, On the rms-radius of the proton, *Phys. Lett. B* **576**, 62 (2003).
- [10] R. Pohl, R. Gilman, G. A. Miller and K. Pachucki, Muonic Hydrogen and the Proton Radius Puzzle, *Annu. Rev. Nucl. Part. Sci.* **63**, 175 (2013).
- [11] A. V. Volotka, V. M. Shabaev, G. Plunien and G. Soff, Zemach and magnetic radius of the proton from the hyperfine splitting in hydrogen, *Eur. Phys. J. D* **33**, 23 (2005).
- [12] A. Dupays, A. Beswick, B. Lepetit, C. Rizzo and D. Bakalov, Proton Zemach radius from measurements of the hyperfine splitting of hydrogen and muonic hydrogen, *Phys. Rev. A* **68**, 052503 (2003).
- [13] S. G. Karshenboim, Model-independent determination of the magnetic radius of the proton from spectroscopy of ordinary and muonic hydrogen, *Phys. Rev. D* **90**, 053013 (2014).
- [14] I. Sick and D. Trautmann, Proton root-mean-square radii and electron scattering, *Phys. Rev. C* **89**, 012201 (2014).
- [15] G. Lee, J. R. Arrington and R. J. Hill, Extraction of the proton radius from electron-proton scattering data, *Phys. Rev. D* **92**, 013013 (2015).
- [16] M. O. Distler, T. Walcher, J. C. Bernauer, Solution of the proton radius puzzle? Low momentum transfer electron scattering data are not enough, *arXiv:1511.00479* (2015).
- [17] B. de Beauvoir, C. Schwob, O. Acef, L. Jozefowski, L. Hilico, F. Nez, L. Julien, A. Clairon and F. Biraben, Metrology of the H and D atoms: Determination of the Rydberg constant and Lamb shifts, *Eur. Phys. J. D* **12**, 61 (2000).
- [18] S. Karshenboim et al., Theory of lamb shift in muonic hydrogen, *J. Phys. Chem. Ref. Data* **44**, 031202 (2015).
- [19] C. Peset and A. Pineda, The Lamb shift in muonic hydrogen and the proton radius from effective field theories, *Eur. Phys. J. A* **51**, 1-19 (2015).
- [20] I. Lorenz, U.-G. Meißner, H.-W. Hammer and Y.-B. Dong, Theoretical constraints and systematic effects in the determination of the proton form factors, *Phys. Rev. D* **91**, 014023 (2015).

- [21] D. W. Higinbotham, A. A. Kabir, V. Lin, D. Meekins, B. Norum and B. Sawatzky, The Proton Radius from Electron Scattering Data, arXiv:1510.01293 (2015).
- [22] K. Griffioen, C. Carlson and S. Maddox, Are Electron Scattering Data Consistent with a Small Proton Radius?, *Phys. Rev. C* **93**, 065207 (2015).
- [23] A. Gasparian, The PRad experiment and the proton radius puzzle, *EPJ Web Conf.* **73**, 07006 (2014).
- [24] M. Mihovilovic, H. Merkel and A. Weber, Puzzling out the proton radius puzzle, *EPJ Web of Conf.* **81**, 01009 (2014).
- [25] R. Gilman, Studying the proton radius puzzle with μp elastic scattering, *AIP Conf. Proc.* **1563** 167 (2013).
- [26] S. G. Karshenboim, D. McKeen and M. Pospelov, Constraints on muon-specific dark forces, *Phys. Rev. D* **90**, 073004 (2014).
- [27] C. E. Carlson, The proton radius puzzle, *Prog. Part. Nucl. Phys.* **82**, 59 (2015).
- [28] U. D. Jentschura, Muonic bound systems, virtual particles, and proton radius, *Phys. Rev. A* **92**, 012123 (2015).
- [29] A. Matveev, C. G. Parthey, K. Predehl, J. Alnis, A. Beyer, R. Holzwarth, T. Udem, T. Wilken, N. Kolachevsky, M. Abgrall, D. Rovera, C. Salomon, P. Laurent, G. Grosche, O. Terra, T. Legero, H. Schnatz, S. Weyers, B. Altschul and T. W. Hänsch, Precision Measurement of the Hydrogen 1S-2S Frequency via a 920-km Fiber Link, *Phys. Rev. Lett.* **110**, 230801 (2013).
- [30] M. Horbatsch and E. A. Hessels, Shifts from a distant neighboring resonance, *Phys. Rev. A* **82**, 052519 (2010).
- [31] A. Beyer, L. Maisenbacher, K. Khabarova, A. Matveev, R. Pohl, T. Udem, T. W. Hänsch and N. Kolachevsky, Precision spectroscopy of 2S-nP transitions in atomic hydrogen for a new determination of the Rydberg constant and the proton charge radius, *Phys. Scr.* **T165**, 014030 (2015).
- [32] S. Galtier, H. Fleurbaey, S. Thomas, L. Julien, F. Biraben and F. Nez, Progress in Spectroscopy of the 1S-3S Transition in Hydrogen, *J. Phys. Chem. Ref. Data* **44**, 031201 (2015).
- [33] A. Vutha, N. Bezginov, I. Ferchichi, M. George, V. Isaac, C. Storry, A. Weatherbee, M. Weel and E. Hessels, Progress towards a new microwave measurement of the hydrogen n=2 Lamb shift: a measurement of the proton charge radius, *Bull. Am. Phys. Soc.* **57**, (2012).
- [34] J. N. Tan, S. M. Brewer and N. D. Guise, Experimental efforts at NIST towards one-electron ions in circular Rydberg states, *Phys. Scr.* **T144**, 014009 (2011).
- [35] D. A. Cooke, P. Crivelli, J. Alnis, A. Antognini, B. Brown, S. Friedreich, A. Gabard, T. W. Hänsch, K. Kirch, A. Rubbia and V. Vrankovic, Observation of positronium annihilation in the 2S state: towards a new measurement of the 1S-2S transition frequency, *Hyperfine Interact.* **233** 67 (2015).
- [36] A. Adamczak, D. Bakalov, L. Stoychev and A. Vacchi, Hyperfine spectroscopy of muonic hydrogen and the PSI Lamb shift experiment, *Nucl. Instr. and Meth.*

- Phys. Res. B* **281**, 72 (2012).
- [37] M. Sato, K. Ishida, M. Iwasaki, S. Kanda, Y. Ma, Y. Matsuda, T. Matsuzaki, K. Midorikawa, Y. Oishi, S. Okada, N. Saito, K. Tanaka, Laser spectroscopy of the hyperfine splitting energy in the ground state of muonic hydrogen. 10.3204/DESY-PROC-2014-04/67 (2014).
 - [38] R. N. Faustov, A. P. Martynenko, G. A. Martynenko and V. V. Sorokin, Radiative nonrecoil nuclear finite size corrections of order $\alpha(Z\alpha)^5$ to the HFS of S-states in μp , *Phys. Lett. B* **733**, 354 (2014).
 - [39] C. E. Carlson, V. Nazaryan and K. Griffioen, Proton-structure corrections to hyperfine splitting in muonic hydrogen, *Phys. Rev. A* **83**, 042509 (2011).
 - [40] F. Hagelstein and V. Pascalutsa, Proton structure in the hyperfine splitting of muonic hydrogen, *arXiv:1511.04301* (2015).
 - [41] F. Hagelstein, R. Miskimen and V. Pascalutsa, Nucleon Polarizabilities: from Compton Scattering to Hydrogen Atom, *Progress in Particle and Nuclear Physics* **88**, 29-97 (2016).
 - [42] M. O. Distler, J. C. Bernauer and T. Walcher, The RMS charge radius of the proton and Zemach moments, *Phys. Lett. B* **696**, 343 (2011).
 - [43] I. Sick, Zemach moments of He^3 and He^4 , *Phys. Rev. C* **90**, 064002 (2014).
 - [44] Z.-T. Lu, P. Mueller, G. W. F. Drake, W. Nörtershäuser, S. C. Pieper and Z.-C. Yan, Laser probing of neutron-rich nuclei in light atoms, *Rev. Mod. Phys.* **85**, 1383 (2013).
 - [45] M. Herrmann, M. Haas, U. D. Jentschura, F. Kottmann, D. Leibfried, G. Saathoff, C. Gohle, A. Ozawa, V. Batteiger, S. Knünz, N. Kolachevsky, H. A. Schüssler, T. W. Hänsch and T. Udem, Feasibility of coherent xuv spectroscopy on the 1S-2S transition in singly ionized helium, *Phys. Rev. A* **79**, 052505 (2009).
 - [46] D. Z. Kandula, C. Gohle, T. J. Pinkert, W. Ubachs and K. S. E. Eikema, XUV frequency-comb metrology on the ground state of helium, *Phys. Rev. A* **84**, 062512 (2011).